Integrated control of ground vehicles dynamics via advanced terminal sliding mode control

Integrated control of ground vehicles dynamics via advanced terminal sliding mode control

Eman Mousavinejad, Qing-Long Han, Fuwen Yang, Yong Zhu and Ljubo Vlacic

School of Engineering, Griffith University, Gold Coast, QLD, Australia

ABSTRACT

An integrated vehicle dynamics control (IVDC) algorithm, developed for improving vehicle handling and stability under critical lateral motions, is discussed in this paper. The IVDC system utilises integral and nonsingular fast terminal sliding mode (NFTSM) control strategies and coordinates active front steering (AFS) and direct yaw moment control (DYC) systems. When the vehicle is in the normal driving situation, the AFS system provides handling enhancement. If the vehicle reaches its handling limit, both AFS and DYC are then integrated to ensure the vehicle stability. The major contribution of this paper is in improving the transient response of the vehicle yaw rate and sideslip angle tracking controllers by implementing advanced types of sliding mode strategies, namely integral terminal sliding mode and NFTSM, in the IVDC system. Simulation results demonstrate that the developed control algorithm for the IVDC system not only has strong robustness against uncertainties but also improves the transient response of the control system.

KEYWORDS

Integrated vehicle dynamics control; direct yaw moment control; active front steering; vehicle stability; terminal sliding mode; transient response

1. Introduction

Vehicle active safety systems have been developed to improve handling characteristics of ground vehicles over the past three decades. The handling characteristics of a vehicle are seen as the vehicle's response to steering commands and also to environmental inputs, such as road disturbances and wind gusts, which have an effect on the vehicle direction of motion [1].

A variety of systems designed for vehicle direction motion control have attracted intensive research attention from both the academia and industry. This type of system-enhancing active safety of vehicles is referred to as a vehicle stability control (VSC) system. For VSC, controlling the lateral dynamics of the vehicle plays an important role when it comes to stabilising the vehicle's lateral motion in severe cornering manoeuvres.

The VSC system has two main types: (i) the active steering (AS) system and (ii) the direct yaw moment control (DYC) system. The AS system assists a driver in improving the vehicle lateral dynamics through the correction of front wheel angles, active front steering (AFS) [2–8]; and rear wheel angles, active rear steering (ARS) [9]. The main problem with

CONTACT Eman Mousavinejad eman.mousavinejad@griffithuni.edu.au

AS systems is that the ability of these systems is drastically reduced in the nonlinear range of lateral tyre forces with respect to tyre sideslip angle (i.e. lateral tyre forces saturation).

In order to stabilise a vehicle in both linear and nonlinear regions of lateral tyre forces, the direct yaw moment control system was developed [10–15]. The DYC system improves the vehicle lateral performance by generating the corrective yaw moment produced by the longitudinal force on the individual tyres. This longitudinal force can be obtained from the active differential braking system. The major deficiency of DYC is that continuous use of the braking force causes the vehicle to slow down significantly, so it has an undesirable effect on the vehicle longitudinal motion.

Recent approaches to the above-discussed problems of the AS and DYC systems [16,17] have suggested that the maximum effectiveness of VSC could be gained through the integrated use of AS and DYC systems, which is referred to as an integrated vehicle dynamics control (IVDC). A comparative study of AFS and ARS coordinated with DYC concludes that AFS is more suitable to be integrated with DYC than ARS, as ARS is an effective method to control the vehicle only at low speed cornering manoeuvres due to the steering angle limitation of rear wheels; however AFS is effective to control the vehicle both in high speed and low speed cornering manoeuvres [18].

Over the past two decades, IVDC systems have been an important research topic in the area of vehicle dynamics and control. Comprehensive reviews on this research field may refer to [19,20] and various robust control techniques have been proposed to achieve the aim of functional integration of vehicle dynamics control systems.

A comparison between the optimal guaranteed cost coordination control method and the optimal coordination scheme based on linear-quadratic regulator theory for integrated AFS and DYC was proposed in [21]. As discussed in [22], sliding mode control (SMC) is implemented for stabilising the forces and moments in an integrated control algorithm which coordinates steering, braking, and stabiliser. Other application aspects of the SMC concept are addressed in [23–25]. To ensure the robustness of integrated AFS and DYC systems, a control algorithm based on linear parameter-varying (LPV) formulation and static-state feedback controller was presented in [26–28]. In [29] a switched model predictive controller and in [30,31] a nonlinear model predictive controller were proposed to coordinate AFS and DYC. An integrated robust model-matching controller was designed in [32] using an H_∞ technique based on linear matrix inequalities. The controller integrates ARS, longitudinal force compensation and active yaw moment controls. The authors in [33] introduced an integrated control strategy involving AFS and DYC based on a gain-scheduled LPV controller for a four-wheel steering vehicle.

In general, a discrepancy always exits between the actual vehicle model and its mathematical model. Therefore, in this paper, vehicle motion is represented as a nonlinear system because of the nonlinearities of tyre forces, vehicle dynamics model uncertainties (i.e. variation of vehicle parameters such as mass, speed, and body moment of inertia), and external disturbance, such as variation of road conditions, which may have an effect on controlling the vehicle motion.

The enhancement of the transient response of the IVDC system is the motivation of the current study so that the vehicle is able to trace the desired motion with the fast performance. The reason for this motivation is the fact that in a real driving condition, the vehicle lateral motion stability in the presence of the system's uncertainties and external disturbance relies heavily on its transient response, so the yaw rate and sideslip angle tracking

controllers should have fast transient responses in the process of reaching their steady-state responses.

In [34], the above-mentioned control strategies for the IVDC system were categorised and compared in terms of control objectives, advantages, and disadvantages. According to Mousavinejad et al. [34], these control techniques are able to track the desired lateral characteristics of a vehicle, yaw rate, and sideslip angle, considering external disturbance and the system's uncertainties. However, they are not effective enough for improving the transient response of the yaw rate and sideslip tracking controllers in the presence of uncertainties and disturbances.

The main contribution of this study is in improving the transient response of the vehicle yaw rate and sideslip angle tracking controllers by implementing two advanced types of sliding mode strategies, namely integral terminal sliding mode (ITSM) and nonsingular fast terminal sliding mode (NFTSM).

The NFTSM control, which provides a fast-finite-time convergence and strong robustness with no singularity issue, was proposed in [35]. NFTSM deals with the second- and higher-order systems. In order to control the class of a first-order system, an ITSM control was introduced in [36]. It is claimed that the proposed ITSM is able to provide a fast-finite-time convergence for a first-order nonlinear system with uncertainties and external disturbance.

The rest of the paper is organised as follows: Section 2 presents a strategy for the IVDC system. The procedure for the design of stand-alone controllers has been addressed in Section 3. Section 4 introduces the integration mechanism for the stand-alone controllers. Sections 5 and 6 are devoted to simulation results and concluding remarks, respectively.

2. The IVDC strategy

In VSC, vehicle yaw rate and body sideslip angle, which is the deviation angle between the vehicle longitudinal velocity and its motion direction, are both critical to control the lateral dynamics of the vehicle [1]. Controlling the yaw rate helps the vehicle to maintain the desired rate and direction of rotation about its vertical axis. However, keeping the vehicle moving along the desired path cannot be obtained just by controlling the yaw rate. For instance, if the tyre–road friction coefficient is small (i.e. slippery road) or if the vehicle speed is high, controlling the yaw rate can only maintain the vehicle in the intended orientation, but the vehicle sideslip angle may increase considerably, causing the vehicle to deviate from its desired path [1]. Therefore, forcing both the yaw rate and sideslip angle to follow their desired values is essential for improving the lateral dynamics behaviour of the vehicle.

According to vehicle lateral dynamics, there are two virtual inputs to control the vehicle, namely lateral force and yaw moment. Therefore, a reference stable region should be chosen for the purpose of controller design. The phase plane method is one of the common strategies for the analysis of a nonlinear system and the determination of a stable region. Referring to [37], there are two types of vehicle phase plane: (i) sideslip angle and yaw rate stable region, and (ii) sideslip angle and sideslip angular velocity stable region. The related study [38] indicates that the second method is superior to the first as, in the strictest sense, sideslip angle against yaw rate is not a phase plane plot and therefore physical interpretation

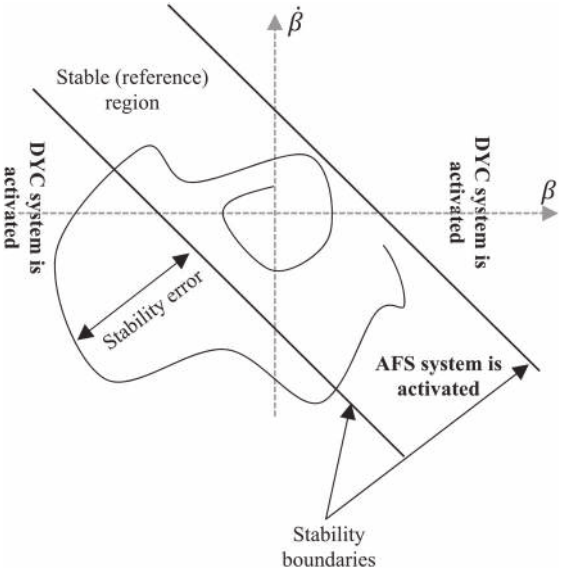

Figure 1. Different regions in the $\beta - \dot{\beta}$ phase plane.

of vehicle behaviour is difficult. The reference region based on the $\beta - \dot{\beta}$ phase plane is illustrated in Figure 1.

The IVDC strategy can be expressed as follows: in order to improve the handling of the vehicle within the reference region, Figure 1, the AFS system generates the corrective yaw moment to force the yaw rate to follow its desired value through adding a corrective angle to the front wheels and minimising the vehicle sideslip angle by controlling the lateral tyre force. When the vehicle states exceed the stability boundaries, Figure 1, the DYC system provides the extra corrective yaw moment to move the vehicle states back to the reference region by controlling the sideslip angle through the activation of the differential braking system and, therefore, the DYC system enhances the vehicle stability.

3. Stand-alone controller design

In this section, the design procedures of the three types of stand-alone controllers are presented. The control design is based on a 2-DOF linear vehicle model, as shown in Figure 2, with small wheel angle and constant vehicle forward speed assumptions [39]. The basic equations of motion for this model are as follows:

$$mV_x(\dot{\beta} + \gamma) = F_y, \tag{1}$$

$$I_{zz}\dot{\gamma} = M_z, \tag{2}$$

where $\gamma = \dot{\psi}$, and M_z and F_y are the required body yaw moment and lateral force, respectively. As discussed in Section 1, stand-alone controllers are designed based on the ITSM and NFTSM methods to ensure the robustness and fast transient response of the control system in the existence of a vehicle's uncertainties and nonlinear characteristics.

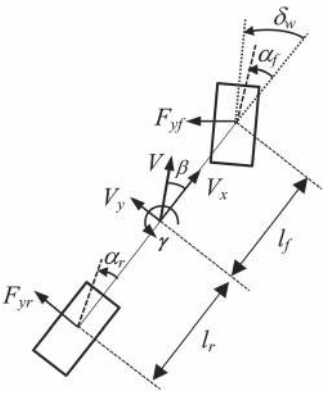

Figure 2. Vehicle bicycle model.

3.1. Sideslip angle and yaw rate desired values

In the steady-state condition, the desired values of the vehicle sideslip angle and yaw rate are expressed as [40]

$$\beta_{\text{des}} = \frac{l_r - \frac{l_f m V_x^2}{2C_r(l_f + l_r)}}{l_f + l_r + V_x^2 k_u}\delta_d, \tag{3}$$

$$\dot{\psi}_{\text{des}} = \gamma_{\text{des}} = \frac{V_x}{(l_f + l_r) + k_u V_x^2}\delta_d, \tag{4}$$

where k_u is the understeer coefficient and is defined *as*

$$k_u = m\left(\frac{l_r C_r - l_f C_f}{2(l_f + l_r)C_f C_r}\right). \tag{5}$$

As mentioned in [40], the friction coefficient of the road is not always able to provide tyre forces to support a high yaw rate. Therefore, the desired values must be bounded by considering the tyre–road friction coefficient, μ. The upper bounds for the sideslip angle and yaw rate are suggested as

$$\beta_{\text{upper\_bound}} = \tan^{-1}(0.02\,\mu g), \tag{6}$$

$$\dot{\psi}_{\text{upper\_bound}} = 0.85\frac{\mu g}{V_x}. \tag{7}$$

3.2. AFS controller for handling

In the handling region, the lateral tyre force is assumed to have a linear function with the tyre slip angle as follows:

$$F_{yf,r} = -2C_{f,r}\alpha_{f,r}, \tag{8}$$

and M_z can be calculated as

$$M_z = l_f F_{yf} - l_r F_{yr}, \tag{9}$$

where α is the tyre slip angle calculated as

$$\alpha_f = \beta + l_f \frac{\gamma}{V_x} - \delta_w, \quad \alpha_r = \beta - l_r \frac{\gamma}{V_x}. \tag{10}$$

From Equations (8) and (10), the lateral tyre force is the function of the front wheel angle in the handling region, so the vehicle sideslip angle can be minimised by correcting the front wheel angle through the AFS system.

From Equation (1), in the handling region, the vehicle sideslip angle, β, with respect to the lateral tyre force, F_y, follows the dynamics of the first-order system. As a result, the ITSM method can be implemented to minimise the sideslip angle. However, from Equation (2), the vehicle yaw angle, ψ, follows the dynamics of the second-order system with respect to the corrective yaw moment. Therefore, the NFTSM method should be used to design the yaw rate tracking controller.

3.2.1. Sideslip angle controller design

Equation (1) can be rewritten as

$$\dot{\tilde{\beta}} = -\gamma + \frac{F_y^*}{mV_x} + g_{\beta 1}, \tag{11}$$

where $\tilde{\beta} = \beta - \beta_{\text{des}}$, and $g_{\beta 1}$, which is an unknown but bounded function to account for uncertainties and disturbance in the actual nonlinear vehicle model, is defined as

$$|g_{\beta 1}| \leq k''_{\beta}, \quad k''_{\beta} > 0. \tag{12}$$

The states of the system are considered as

$$\begin{aligned} x_1 &= \tilde{\beta}, \\ x_2 &= \dot{x}_1 = \dot{\tilde{\beta}}. \end{aligned} \tag{13}$$

From [36], the ITSM surface can be chosen as

$$s_{\beta 1} = \tilde{\beta} - \tilde{\beta}(0) + \int_0^t \left(\frac{\alpha''_{\beta}}{2} \tilde{\beta} + \frac{\beta''_{\beta}}{2^{\gamma''_{\beta}}} \tilde{\beta}^{\gamma''_{\beta}} \right) \mathrm{d}t, \tag{14}$$

where $\tilde{\beta}(0) = 0$. Therefore, F_y^*, as a control input, is expressed as

$$F_y^* = -mV_x \left(\frac{\alpha''_{\beta}}{2} \tilde{\beta} + \frac{\beta''_{\beta}}{2^{\gamma''_{\beta}}} \beta^{\gamma''_{\beta}} - \gamma + \frac{\alpha''_{\beta}}{2} s_{\beta 1} + \frac{\beta''_{\beta}}{\sqrt{2}} \operatorname{sgn} s_{\beta 1} + k''_{\beta} \operatorname{sgn} s_{\beta 1} \right). \tag{15}$$

Proof: Defining a Lyapunov function as

$$V_1 = \tfrac{1}{2} s_{\beta 1}^2. \tag{16}$$

Differentiating V_1 with respect to time yields

$$\begin{aligned} \dot{V}_1 = s_{\beta 1}\dot{s}_{\beta 1} &= s_{\beta 1}\left(\dot{\tilde{\beta}} + \frac{1}{2}\alpha''_{\beta}\tilde{\beta} + \frac{\beta''_{\beta}}{2^{\gamma''_{\beta}}}\tilde{\beta}^{\gamma''_{\beta}}\right) \\ &= s_{\beta 1}\left(-\gamma + \frac{F_y^*}{mV_x} + g_{\beta 1} + \frac{\alpha''_{\beta}}{2}\tilde{\beta} + \frac{\beta''_{\beta}}{2}\tilde{\beta}^{\gamma''_{\beta}}\right). \end{aligned} \tag{17}$$

From Equation (15), it follows that

$$\dot{V}_1 = -k''_{\beta}|s_{\beta 1}| + g_{\beta 1}s_{\beta 1} - \frac{\alpha''_{\beta}}{2}s_{\beta 1}^2 - \frac{\beta''_{\beta}}{\sqrt{2}}|s_{\beta 1}|, \tag{18}$$

$$\dot{V}_1 \le -k''_{\beta}|s_{\beta 1}| + |g_{\beta 1}||s_{\beta 1}| - \frac{\alpha''_{\beta}}{2}s_{\beta 1}^2 - \frac{\beta''_{\beta}}{\sqrt{2}}|s_{\beta 1}|. \tag{19}$$

Since $|g_{\beta 1}| \le k''_{\beta}$, we have

$$\dot{V}_1 \le -\frac{\alpha''_{\beta}}{2}s_{\beta 1}^2 - \frac{\beta''_{\beta}}{\sqrt{2}}|s_{\beta 1}|, \tag{20}$$

$$\dot{V}_1 \le -\alpha''_{\beta}V_1 - \beta''_{\beta}V_1^{1/2} \Rightarrow \dot{V}_1 \le 0. \tag{21}$$

Equation (21) is the sufficient condition for the system states to converge equilibrium points in the fast-finite-time on the ITSM surface.

Finally, from Equations (8) and (10), the sideslip-controlled front wheel angle can be derived as

$$\delta_{w\beta} = \frac{1}{2C_f}\left(F_y^* + 2(C_f + C_r)\beta - \frac{2(l_rC_r - l_fC_f)}{V_x}\gamma\right). \tag{22}$$

■

3.2.2. Yaw rate controller design

Equation (2) can be expressed as

$$\dot{\tilde{\gamma}} = \ddot{\tilde{\psi}} = \frac{1}{I_{zz}}M_{\mathrm{AFS}} + g_{\psi}, \tag{23}$$

where M_{AFS} is the corrective yaw moment to improve the vehicle handling, $\tilde{\gamma} = \gamma - \gamma_{\mathrm{des}}$, and g_{ψ} is an unknown-bounded function satisfying the following equation as

$$|g_{\psi}| \le k'_{\psi 1}, \quad k'_{\psi 1} > 0. \tag{24}$$

The system states are chosen as

$$\begin{aligned} x_1 &= \tilde{\psi}, \\ x_2 &= \dot{x}_1 = \dot{\tilde{\psi}} = \tilde{\gamma}. \end{aligned} \tag{25}$$

From [35], the NFTSM surface can be defined as

$$s_\psi = \tilde{\psi} + \alpha'_\psi |\tilde{\psi}|^{\gamma_{\psi 1}} \operatorname{sgn} \tilde{\psi} + \beta'_\psi |\dot{\tilde{\psi}}|^{\gamma_{\psi 2}} \operatorname{sgn} \dot{\tilde{\psi}}. \tag{26}$$

Then M_{AFS}, as a control input, is rewritten as

$$M_{\mathrm{AFS}} = -I_{zz} \left(\frac{1}{\beta'_\psi \gamma_{\psi 2}} |\dot{\tilde{\psi}}|^{2-\gamma_{\psi 2}} \operatorname{sgn} \dot{\tilde{\psi}} (1 + \alpha' \psi \gamma_{\psi 1} |\tilde{\psi}|^{\gamma_{\psi 1}-1}) + k'_{\psi 1} \operatorname{sgn} s_\psi + k'_{\psi 2} s_\psi \right). \tag{27}$$

Proof: Consider a Lyapunov candidate as

$$V_2 = \frac{1}{2} s_\psi^2. \tag{28}$$

The time derivative of the Lyapunov candidate is obtained as

$$\dot{V}_2 = s_\psi \dot{s}_\psi = s_\psi (\dot{\tilde{\psi}} + \alpha'_\psi \gamma_{\psi 1} |\tilde{\psi}|^{\gamma_{\psi 1}-1} \dot{\tilde{\psi}} + \beta'_\psi \gamma_{\psi 2} |\dot{\tilde{\psi}}|^{\gamma_{\psi 2}-1} \ddot{\tilde{\psi}}). \tag{29}$$

By substituting $\ddot{\tilde{\psi}}$ from Equation (23) and M_{AFS} from Equation (27) into Equation (29), we have

$$\dot{V}_2 = s_\psi (\beta'_\psi \gamma_{\psi 2} |\dot{\tilde{\psi}}|^{\gamma_{\psi 2}-1} g_\psi - k'_{\psi 1} \beta'_\psi \gamma_{\psi 2} |\dot{\tilde{\psi}}|^{\gamma_{\psi 2}-1} \operatorname{sgn} s_\psi - k'_{\psi 2} \beta'_\psi \gamma_{\psi 2} |\dot{\tilde{\psi}}|^{\gamma_{\psi 2}-1} s_\psi). \tag{30}$$

As $|g_\psi| \leq k'_{\psi 1}$, it can be concluded that

$$\dot{V}_2 \leq -k'_{\psi 2} \beta'_\psi \gamma_{\psi 2} |\dot{\tilde{\psi}}|^{\gamma_{\psi 2}-1} s_\psi^2, \tag{31}$$

$$\dot{V}_2 \leq -2k'_{\psi 2} \beta'_\psi \gamma_{\psi 2} |\dot{\tilde{\psi}}|^{\gamma_{\psi 2}-1} V_2 \Rightarrow \dot{V}_2 \leq 0. \tag{32}$$

Therefore, the system can satisfy the Lyapunov stability condition and the system states will reach the NFTSM surface within the fast-finite-time.

From Equations (8) to (10), the yaw rate-controlled front wheel angle is found as

$$\delta_{w\psi} = \frac{1}{2 l_f C_f} \left(M_{\mathrm{AFS}} - 2(l_r C_r - l_f C_f)\beta + \frac{2(l_f^2 C_f + l_r^2 C_r)}{V_x} \gamma \right). \tag{33}$$

Hence, the front wheel angle generated by the AFS system is a combination of $\delta_{w\beta}$ and $\delta_{w\psi}$ as

$$\delta_w = w_1 \delta_{w\psi} + w_2 \delta_{w\beta}, \tag{34}$$

where w_1 and w_2 are the weighting coefficients and determined through trial and error. The term M_{AFS} in Equation (33) has to be replaced with the term $M^*_{\mathrm{AFS}} = \rho M_{\mathrm{AFS}}$, where ρ is the adaption gain introduced in Section 4, in order to consider the adaption gain used for integration of the steering system and braking system. ■

3.3. DYC controller for stability

The DYC system employs the body yaw moment to control the sideslip angle. To obtain the body yaw moment, M_{DYC}, for the sideslip angle control, differentiating Equation (1) and substituting into Equation (2) for $\dot{\gamma}$ result in the following expression:

$$\ddot{\tilde{\beta}} = -\frac{M_{\mathrm{DYC}}}{I_{zz}} + \frac{\dot{F}_y}{mV_x} + g_{\beta 2}, \tag{35}$$

where M_{DYC} is the control input, $\dot{F}_y$ is the derivative of the body lateral force, and $g_{\beta 2}$ is an unknown-bounded function as

$$|g_{\beta 2}| \leq k'_{\beta 1}, \quad k'_{\beta 1} > 0. \tag{36}$$

3.3.1. Sideslip angle controller design

Since the sideslip angle outside the handling region follows the dynamics of the second-order system with respect to M_{DYC}, the NFTSM strategy is applied to control the system. The states of the system are as

$$\begin{aligned} x_1 &= \tilde{\beta}, \\ x_2 &= \dot{x}_1 = \dot{\tilde{\beta}}. \end{aligned} \tag{37}$$

According to [35], the NFTSM surface can be considered as

$$s_{\beta 2} = \tilde{\beta} + \alpha'_{\beta} |\tilde{\beta}|^{\gamma_{\beta 1}} \operatorname{sgn} \tilde{\beta} + \beta'_{\beta} |\dot{\tilde{\beta}}|^{\gamma_{\beta 2}} \operatorname{sgn} \dot{\tilde{\beta}}. \tag{38}$$

So, M_{DYC}, as a control input, can be found as

$$M_{\mathrm{DYC}} = I_{zz} \left(\frac{1}{\beta'_{\beta} \gamma_{\beta 2}} |\dot{\tilde{\beta}}|^{2-\gamma_{\beta 2}} \operatorname{sgn} \dot{\tilde{\beta}} (1 + \alpha'_{\beta} \gamma_{\beta 1} |\tilde{\beta}|^{\gamma_{\beta 1}-1}) + k'_{\beta 1} \operatorname{sgn} s_{\beta 2} + k'_{\beta 2} s_{\beta 2} \right). \tag{39}$$

Remark 3.1: The actual sideslip angle can be estimated by using the lateral acceleration sensor, speed sensor, and yaw rate sensor based on the following equation:

$$\dot{\beta} = \frac{a_y}{V_x} - \gamma. \tag{40}$$

The sideslip angle estimator is not discussed in this paper and can be found in [41].

Remark 3.2: The Lyapunov stability proof of the DYC control system is omitted as it is similar to the yaw rate NFTSM controller for the AFS system.

3.3.2. DYC system actuator

The differential braking system shown in Figure 3 can be employed as an actuator to generate the corrective yaw moment commanded by the DYC system [12].

According to [12], the brake torques can be calculated from the corrective yaw moment, Equation (39), as follows:

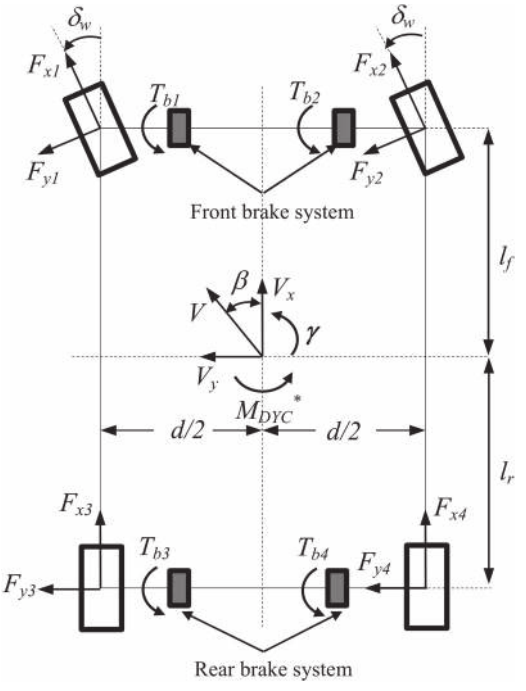

Figure 3. Differential braking system [12].

In understeer condition: when a vehicle is turning counter-clockwise, the brake rear left wheel is activated.

$$M_{\mathrm{DYC}} = \frac{d}{2}F_{x3} = \frac{d}{2}\frac{T_{b3}}{R_w}; \rightarrow T_{b3} = \frac{2R_w}{d}M_{\mathrm{DYC}}, \tag{41}$$

when a vehicle is turning clockwise, the brake rear right wheel is activated.

$$M_{\mathrm{DYC}} = \frac{d}{2}F_{x4} = \frac{d}{2}\frac{T_{b4}}{R_w}; \rightarrow T_{b4} = \frac{2R_w}{d}M_{\mathrm{DYC}}. \tag{42}$$

In oversteer condition: when a vehicle is turning counter-clockwise, the brake front right wheel is activated.

$$M_{\mathrm{DYC}} = \left(\frac{d}{2}\cos\delta_w - l_f \sin\delta_w\right)\frac{T_{b2}}{R_w}; \rightarrow T_{b2} = \frac{R_w}{\left(\frac{d}{2}\cos\delta_w - l_f\sin\delta_w\right)}M_{\mathrm{DYC}}, \tag{43}$$

when a vehicle is turning clockwise, the brake front left wheel is activated.

$$M_{\mathrm{DYC}} = \left(\frac{d}{2}\cos\delta_w - l_f \sin\delta_w\right)\frac{T_{b1}}{R_w}; \rightarrow T_{b1} = \frac{R_w}{\left(\frac{d}{2}\cos\delta_w - l_f\sin\delta_w\right)}M_{\mathrm{DYC}}. \tag{44}$$

The term M_{DYC} has to be replaced with the term M^*_{DYC} in all braking torques $(T_{b1}, T_{b2}, T_{b3}, T_{b4})$ in order to consider the adaption gain used for integration of the

steering system and braking system.

$$M^*_{\mathrm{DYC}} = (1-\rho)M_{\mathrm{DYC}}, \tag{45}$$

where ρ is the adaption gain, which will be introduced in Section 4.

4. Integration of AFS and DYC controllers into IVDC

A coordination mechanism of the AFS and DYC controllers determines which controllers are expected to be used in each region. As discussed earlier, the brake-based DYC technique is not desirable to control the vehicle lateral motion in the reference (stable) region because this technique imposes a direct influence on the longitudinal motion and so reduces the vehicle speed. As a result, the use of the DYC system should be restricted to outside the stable region where the vehicle goes towards instability. The boundaries of the stable region in Figure 1 are defined as [42]

$$\chi = \left| \frac{1}{24}\dot{\beta} + \frac{4}{24}\beta \right| < 1, \tag{46}$$

where χ is the stability index.

Inside the reference (stable) region of the $\beta - \dot{\beta}$ phase plane, improvement of vehicle handling is the main control aim. In this region, the lateral force and body yaw moment, obtained in Equations (15) and (27), are utilised to minimise the sideslip angle and to control the vehicle yaw rate, respectively, through the AFS system. As the vehicle states move beyond the stability control boundaries, lateral tyre forces are saturated, and therefore the AFS system is no longer able to control the sideslip motion. Since the vehicle stability directly depends on the sideslip angle, in this unstable area, the control objective transits from handling to stability and the DYC system is required to stabilise the vehicle by using the extra corrective yaw moment, Equation (39). Consequently, the final body yaw moment is calculated as

$$M^*_z = \rho M_{\mathrm{AFS}} + (1-\rho)M_{\mathrm{DYC}}, \tag{47a}$$

$$M^*_z = M^*_{\mathrm{AFS}} + M^*_{\mathrm{DYC}}, \tag{47b}$$

where $M^*_{\mathrm{AFS}} = \rho M_{\mathrm{AFS}}$, $M^*_{\mathrm{DYC}} = (1-\rho)M_{\mathrm{DYC}}$, and ρ is the adaption gain which is defined according to the vehicle dynamics behaviour in the $\beta - \dot{\beta}$ phase plane, as shown in Figure 4.

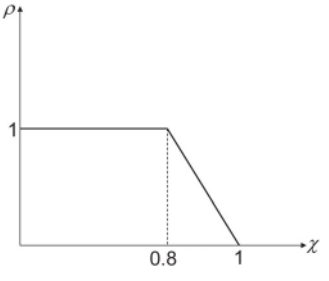

Figure 4. Adaption gain for the integrated AFS and DYC control objects [42].

5. Simulation results and discussions

To evaluate the performance of the proposed IVDC-incorporated SbW and differential braking systems, a series of computer simulations are performed with the MATLAB/SIMULINK software. An 8-DOF nonlinear vehicle model, which is described and validated in [7], with PACEJKA combined slip tyre model [43], is utilised for this purpose.

One of the typical emergency driving manoeuvres for the vehicle lateral stability test is the double lane change (DLC) under different road conditions, i.e. different tyre–road friction coefficients (μ). Therefore, this manoeuvre is implemented to analyse the dynamics behaviour of the vehicle equipped with the designed IVDC system.

Another critical driving manoeuvre is the step steer manoeuvre by which the steady state and transient behavioural response of the vehicle can be evaluated. So, this manoeuvre is conducted to compare the results of the conventional SMC and NFTSM strategies to control the vehicle yaw rate in terms of fast transient response of the control system in the existence of system's uncertainties and external disturbance. The suggested control structure used for simulation is illustrated in Figure 5. The steering wheel controller design with the driver in the loop is not discussed in this study and can be referred from [7].

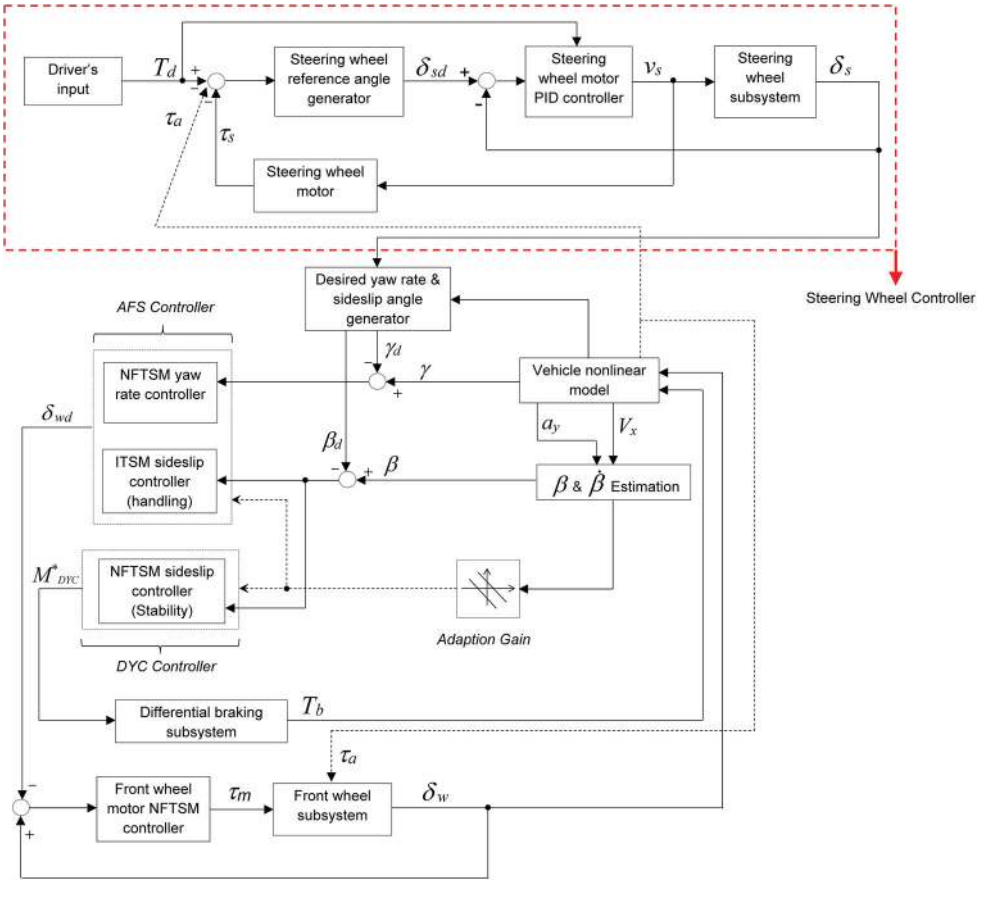

Figure 5. Control structure block diagram.

From this control structure block diagram, the desired values (β_d, γ_d) are calculated by Equations (3) and (4) and compared with their actual values obtained from the sideslip angle estimator and yaw rate sensor, respectively. Following that, the difference between the yaw rate and its desired value is considered as the input of the AFS controller to find the yaw rate-controlled front wheel angle by Equations (23)–(33). At the same time, the stability index, Equation (46), is calculated to determine the stability boundaries for the vehicle trajectory in the $\beta - \dot{\beta}$ phase plane. According to the area of the vehicle trajectory, inside or outside the stable region, the difference between the estimated sideslip angle and its desired value is considered as either the input of the AFS controller to find the sideslip-controlled front wheel angle by Equations (11)–(22) or the input of the DYC controller to calculate the corrective yaw moment M^*_{DYC} through Equations (35)–(39), and (45).

Finally, the total corrective front wheel angle δ_w and yaw moment M^*_{DYC} are exerted to the AFS and DYC actuators, respectively. The SbW front wheel motor controller produces the required motor torque to generate the AFS-commanded front wheel angle through the SbW front wheel subsystem [44]. Moreover, the differential braking system generates the braking torque for each wheel based on the understeer or oversteer condition through Equations (41)–(45).

5.1. DLC manoeuvre

In this manoeuvre, the vehicle moves with an initial speed of 105 km/h on a dry road ($\mu = 0.9$) and 80 km/h on a wet road ($\mu = 0.5$). The driver's commanded front wheel angle providing the DLC manoeuvre is shown in Figure 6. The vehicle parameter uncertainties can be considered as the variation of the vehicle mass and moment of inertia from the unladen to the laden condition (Tables 1–3).

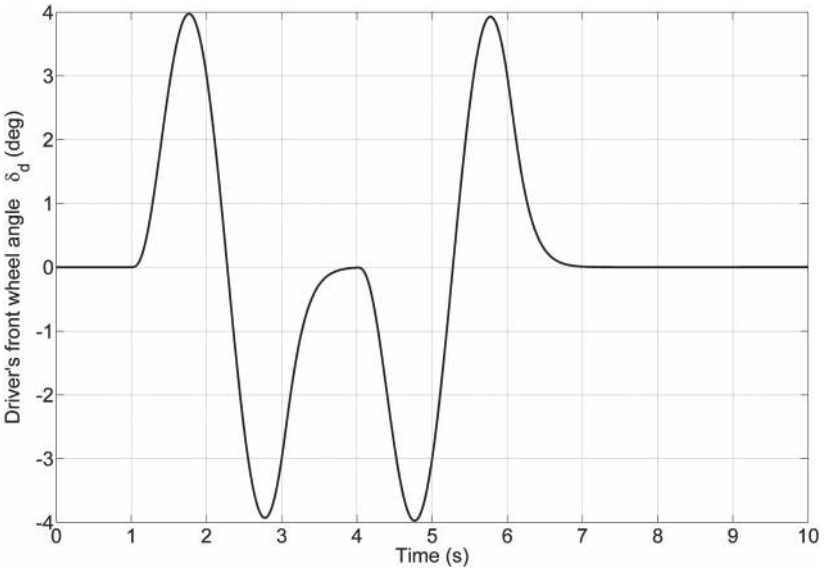

Figure 6. Steering wheel angle commanded by driver.

Table 1. Vehicle parameters.

Symbol	Value
m (unladen)	1300 kg
m (laden)	1600 kg
l_f (unladen)	1.2247 m
l_f (laden)	1.315 m
l_r (unladen)	1.4373 m
l_r (laden)	1.347 m
D	1.4376 m
I_{zz} (unladen)	1808.8 kg m^2
I_{zz} (laden)	1991 kg m^2
R_w	0.285 m
C_f, C_r (dry road)	40,000, 40,000 N/rad
C_f, C_r (wet road)	22,250, 22,250 N/rad

Table 2. Controllers' parameters.

Symbol	Value
α''_β	50
β''_β	0.045
γ''_β	0.6
k''_β	0.05
α'_ψ	2.1
β'_ψ	0.009
$\gamma_{\psi 1}$, $\gamma_{\psi 2}$	1.305, 1.285
$k'_{\psi 1}$, $k'_{\psi 2}$	0.001, 1.5
α'_β	2.1
β'_β	1.2
$\gamma_{\beta 1}$, $\gamma_{\beta 2}$	1.305, 1.285
$k'_{\beta 1}$, $k'_{\beta 2}$	1.6, 1.5
α'_w	20
β'_w	0.005
γ_{w1}, γ_{w2}	1.305, 1.285
k'_{w1}, k'_{w2}	0.02, 0.01

Table 3. Parameters' and variables' definitions.

Symbol	Definition
m	Vehicle total mass
l_f, l_r	Distance from (front, rear) axle to vehicle's centre of gravity
D	Wheel track width
I_{zz}	Vehicle yaw moment of inertia
V_x	Vehicle longitudinal speed
a_y	Vehicle lateral acceleration
μ	Tyre–road friction coefficient
R_w	Effective wheel rolling radius
ψ	Yaw angle
γ	Yaw rate
C_f, C_r	Front, rear tyre cornering stiffness
α_f, α_r	Front, rear tyre sideslip
F_{yf}, F_{yr}	Front, rear lateral tyre force
δ_d	Driver's front wheel angle
δ_w	AFS front wheel angle

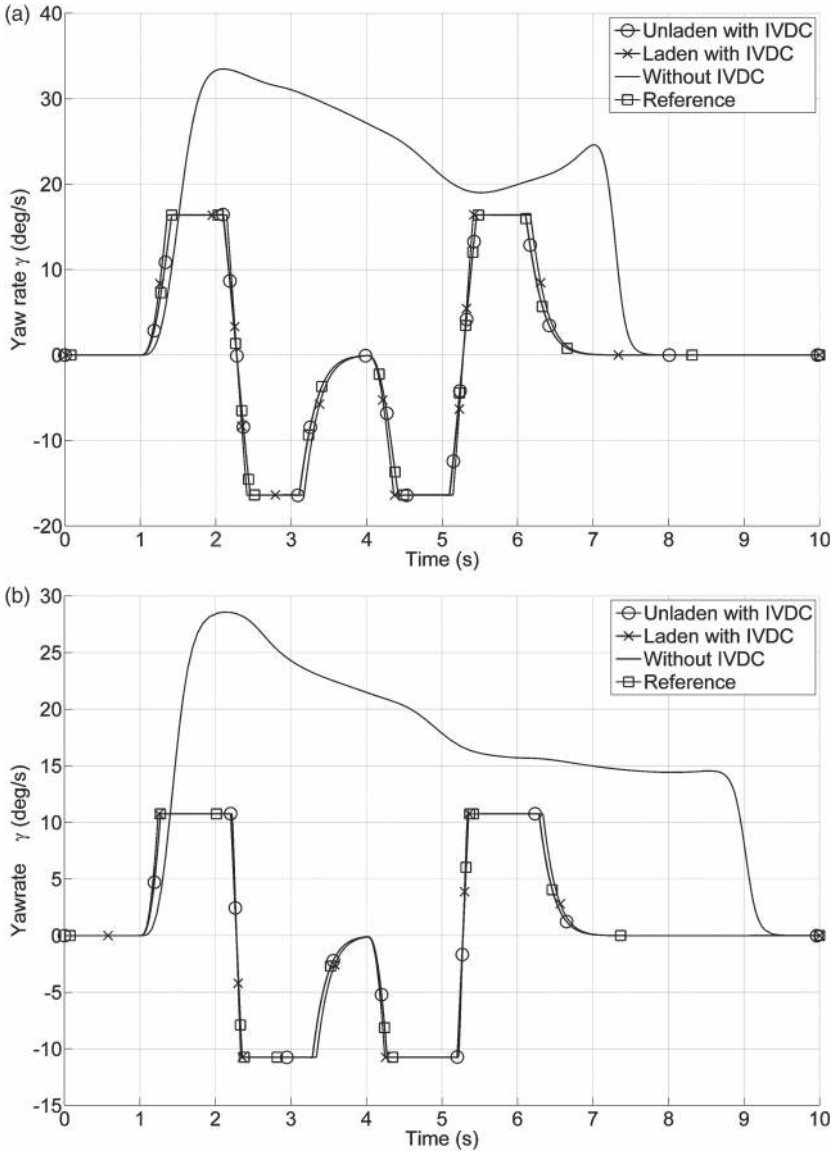

Figure 7. (a) Vehicle yaw rate – dry road. (b). Vehicle yaw rate – wet road.

Figure 7 illustrates the vehicle yaw rate response. The yaw rate of the controlled vehicle could always follow the desired value; while for the uncontrolled vehicle, the absolute value of the yaw rate is always larger than the absolute value of the desired value causing the vehicle to be oversteered.

As shown in Figure 8, the sideslip angle for the controlled vehicle remains between the upper and lower bounds (10° and 4° for dry and wet road conditions, respectively) during the whole manoeuvre, but the uncontrolled vehicle sideslip angle increases significantly; as a result the vehicle loses its stability.

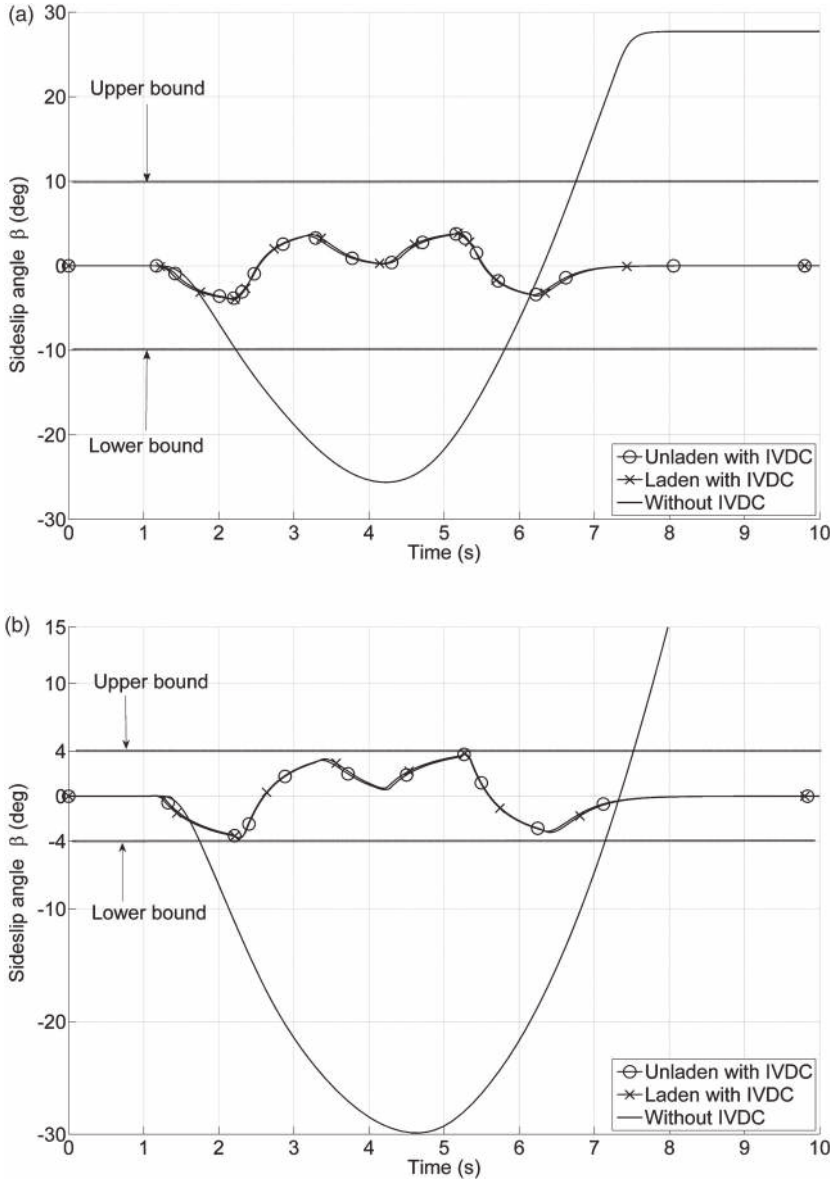

Figure 8. (a) Vehicle body sideslip angle – dry road. (b). Vehicle body sideslip angle – wet road.

The increases in the yaw rate and sideslip angle result in the high lateral acceleration for the uncontrolled vehicle, as depicted in Figure 9. Therefore, the longitudinal speed is reduced and the lateral speed is increased in order to generate this large amount of lateral acceleration, as demonstrated in Figures 10 and 11, respectively.

Having high lateral acceleration and becoming oversteered and unstable lead the uncontrolled vehicle to deviate from the desired path. However, the stable-controlled vehicle covers the desired path well, as depicted in Figure 12.

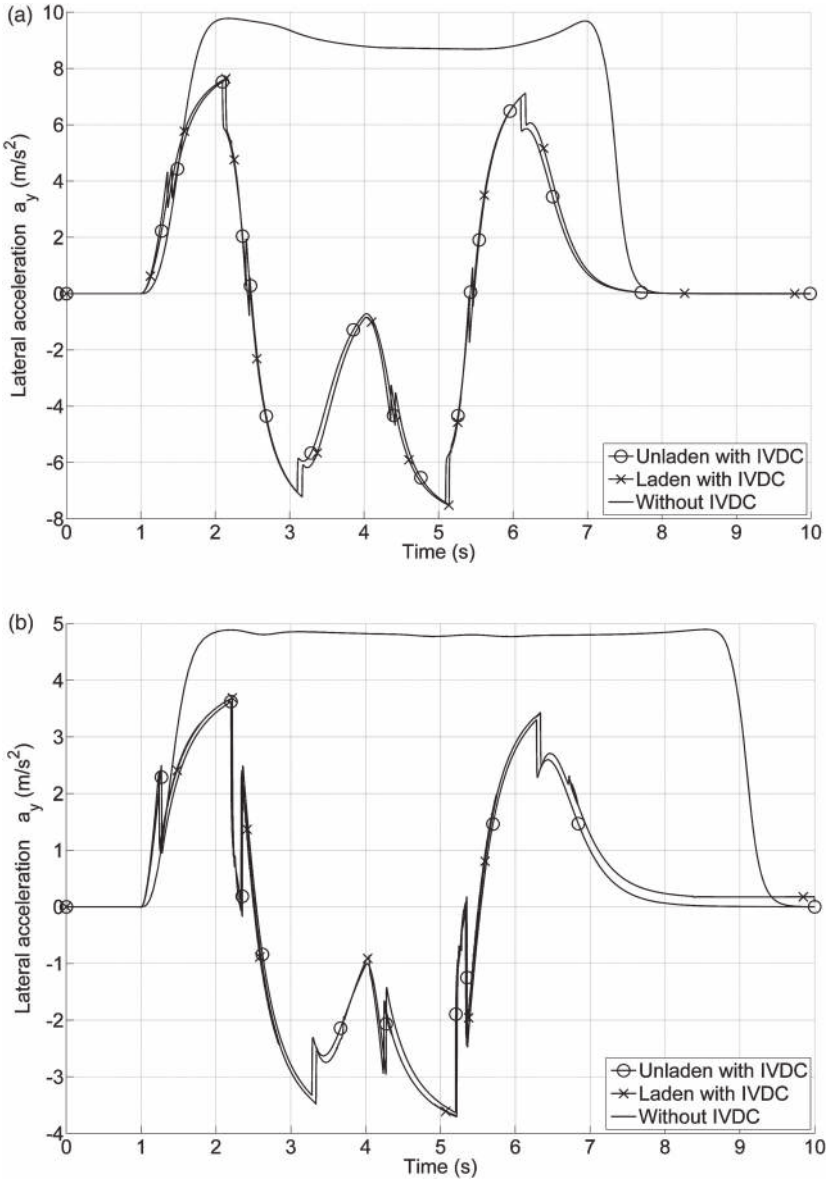

Figure 9. (a) Vehicle lateral acceleration – dry road. (b). Vehicle lateral acceleration – wet road.

Figure 13 shows how the stability index, the dependency parameter, ρ, and generated corrective yaw moment, M^*_{DYC}, evolve according to the driving situations. From Equation (47a) and Figure 13, when the stability index, χ, is below 0.8, the parameter ρ is equal to 1 and so, only AFS is involved in improving the handling performances. However, when χ exceeds 0.8, the parameter ρ is less than 1 and therefore DYC acts in addition to AFS to keep the vehicle stable.

Similarity between the yaw rate amount and covered path in the laden and unladen vehicles indicates the robustness of the proposed control strategy against the vehicle

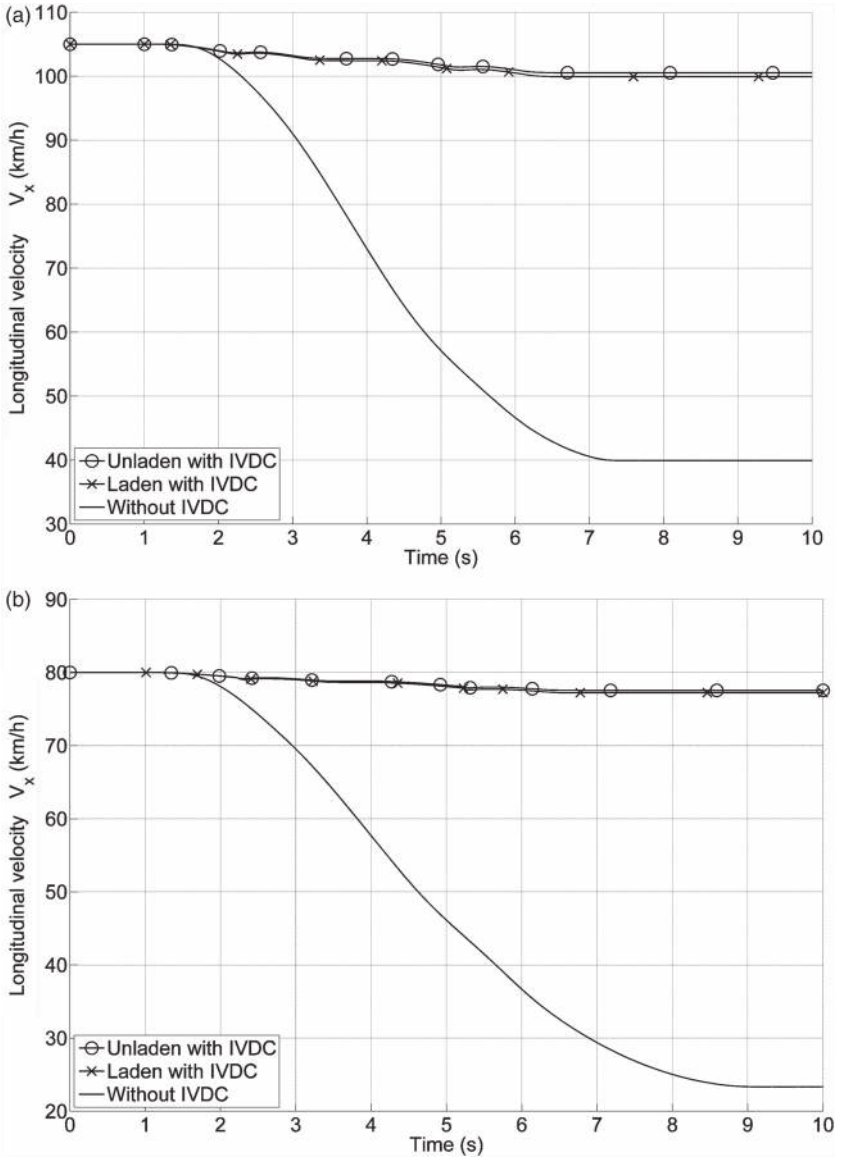

Figure 10. (a) Vehicle longitudinal velocity – dry road. (b). Vehicle longitudinal velocity – wet road.

parameters' uncertainties (i.e. vehicle mass and moment of inertia). In addition, the capability of the control scheme to stabilise the vehicle in the various types of road (i.e. various road–tyre friction coefficients (μ) for dry and wet road conditions) proves the robustness against this uncertain parameter.

In Figure 14, after the trajectory of the controlled vehicle left the stable region, it is attracted again to this area immediately due to the efficiency of the proposed DYC system. However, the trajectory of the uncontrolled vehicle leaves the stable region and it never returns to this area.

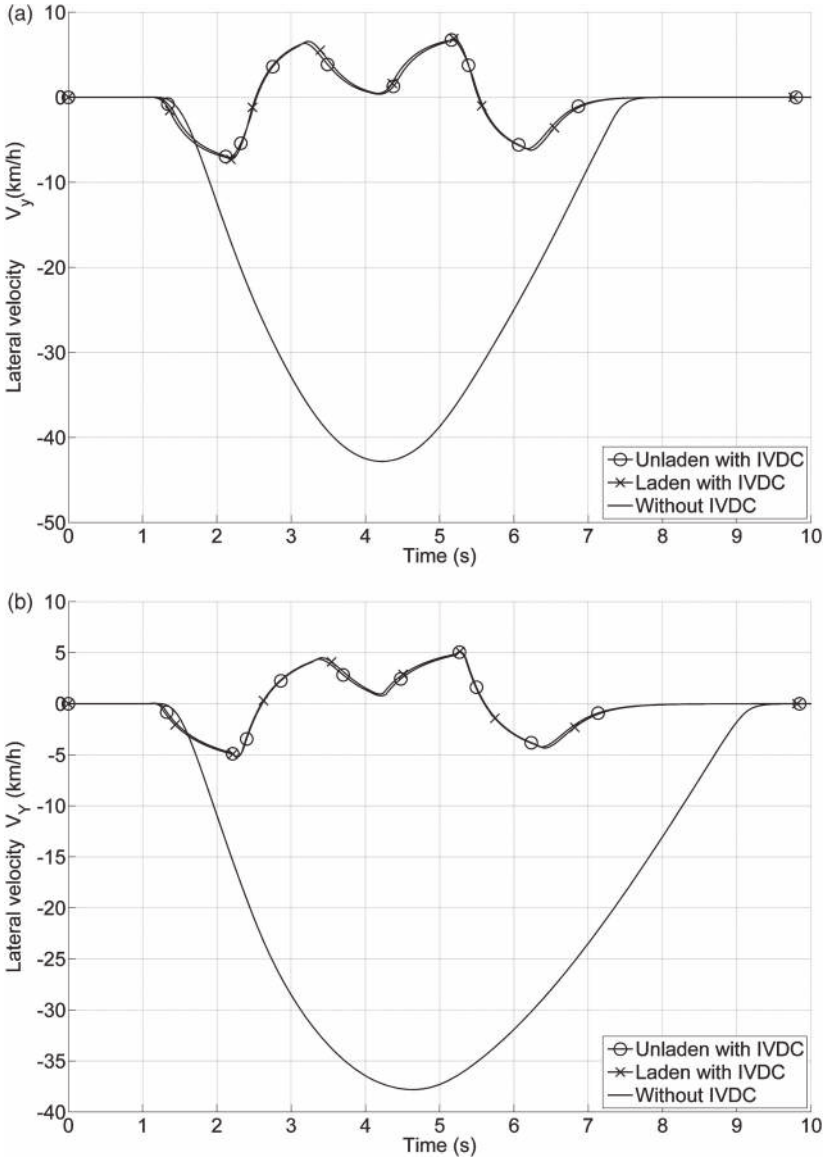

Figure 11. (a) Vehicle lateral velocity – dry road. (b). Vehicle lateral velocity – wet road.

To assess how the proposed IVDC has employed the available subsystems, AFS and DYC, the corrective front wheel angle, $\delta_{wc} = \delta_w - \delta_d$, can be referred from [44] and the corrective yaw moment, M^*_{DYC}, is plotted in Figure 15.

In order to provide the corrective yaw moment commanded by the DYC system, the differential braking system produces the braking torque for each wheel. In a DLC manoeuvre under dry and wet road conditions, as the vehicle is intended to be oversteered, only the front wheels' braking systems are actuated, as illustrated in Figures 16 and 17, and the braking torques for the rear wheels are equal to zero during the whole simulation time. As the braking torques exceed their physical limits, i.e. 907.725 N m (unladen) and 1006.506 N m

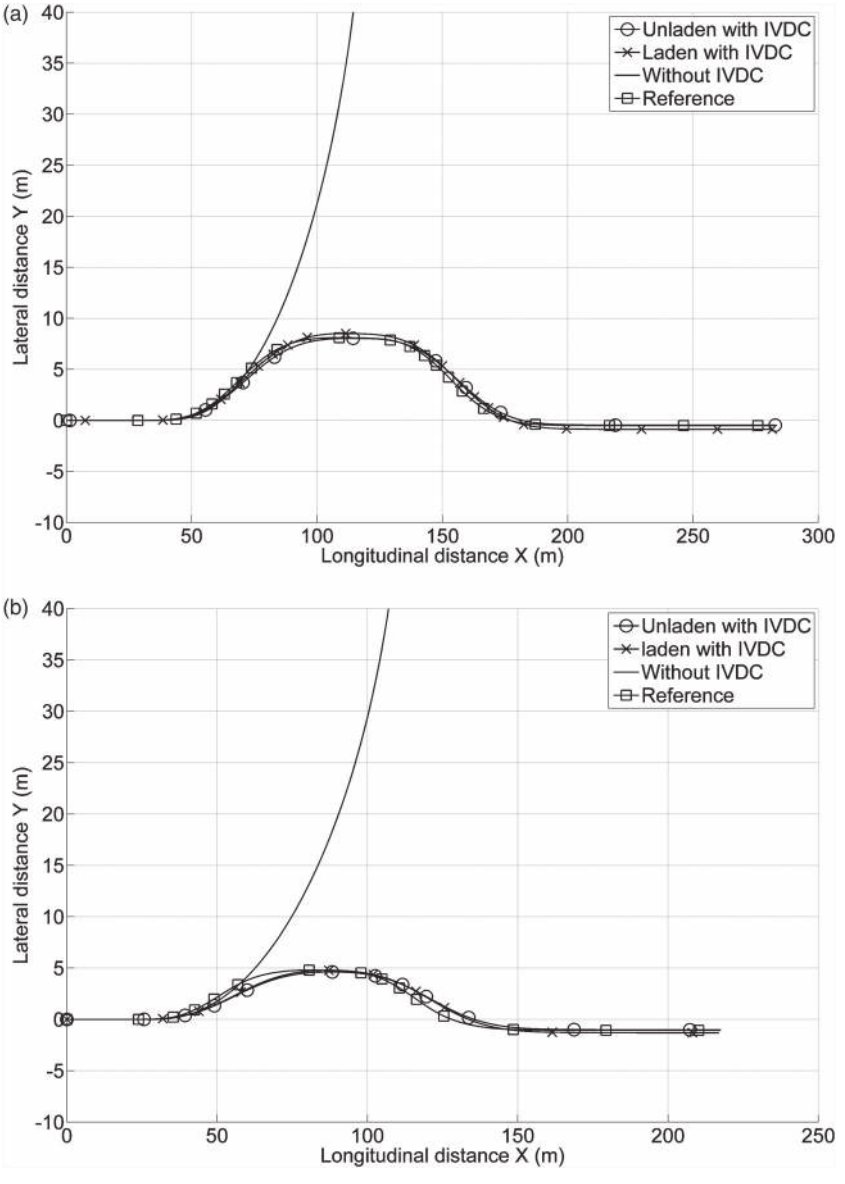

Figure 12. (a) Vehicle trajectory – dry road. (b). Vehicle trajectory – wet road.

(laden) on dry roads and 363.09 N m (unladen), and 446.86 N m (laden) on wet roads, an anti-lock brake system (ABS) should be implemented in order to avoid the tyres being locked. Implementation of ABS is considered as the future work of this study.

5.2. Step steer manoeuvre

Being NFTSM's internal controller, the ITSM controller minimises the vehicle sideslip angle and also this controller assists the yaw rate NFTSM controller to follow its desired

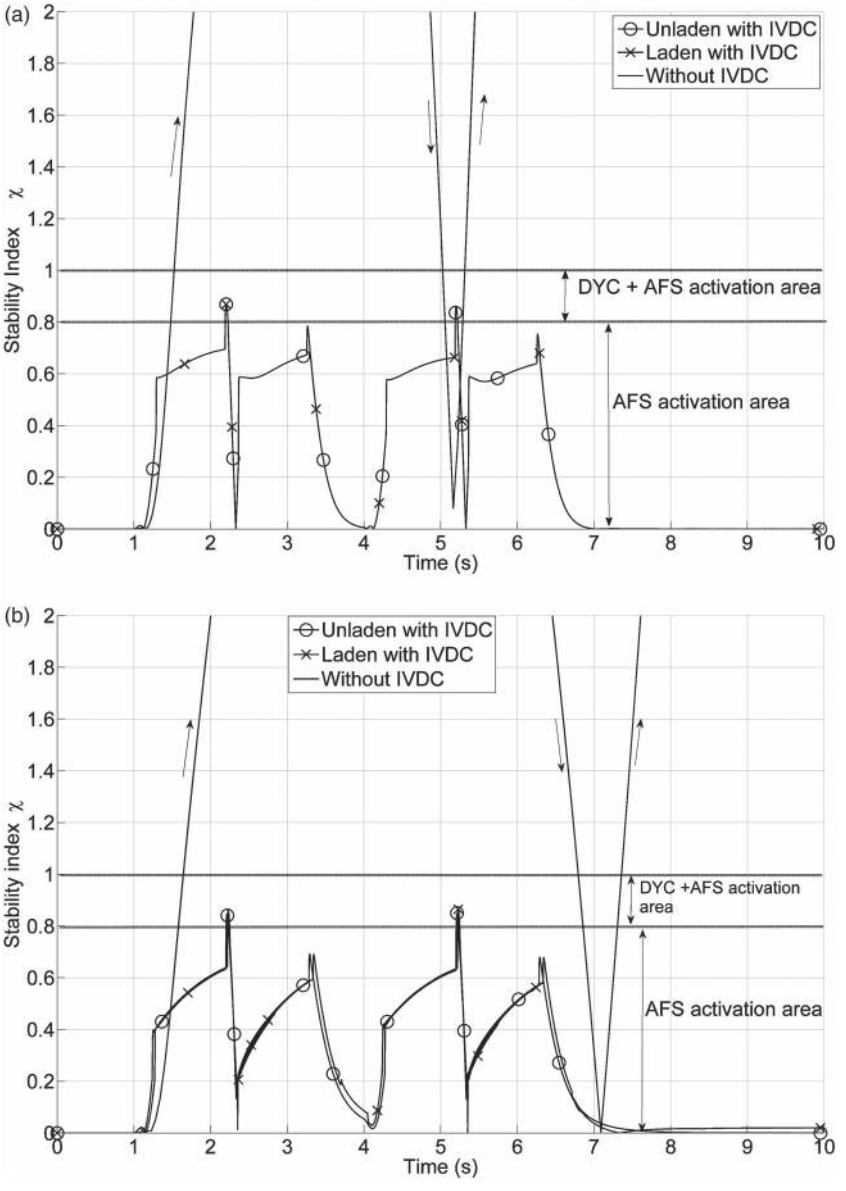

Figure 13. (a) Stability index – dry road. (b). Stability index – wet road.

value in the handling region with the fast transient response. Therefore, the effect of the sideslip ITSM controller can be considered as the overall performance of the yaw rate NFTSM controller and it cannot be evaluated separately.

In order to compare the transient response of the conventional SMC and NFTSM strategies, the performances of these two methods to control the yaw rate of the vehicle are evaluated by inserting a step steering input of 125° to the steering wheel. The vehicle moves at a speed of 80 km/h on a split−μ road surface, where the left side of the vehicle is on a wet road and the right side is on a dry road. As plotted in Figure 18, the yaw rate controller transient response based on the SMC method has an overshoot of about 3°/s and then reaches a

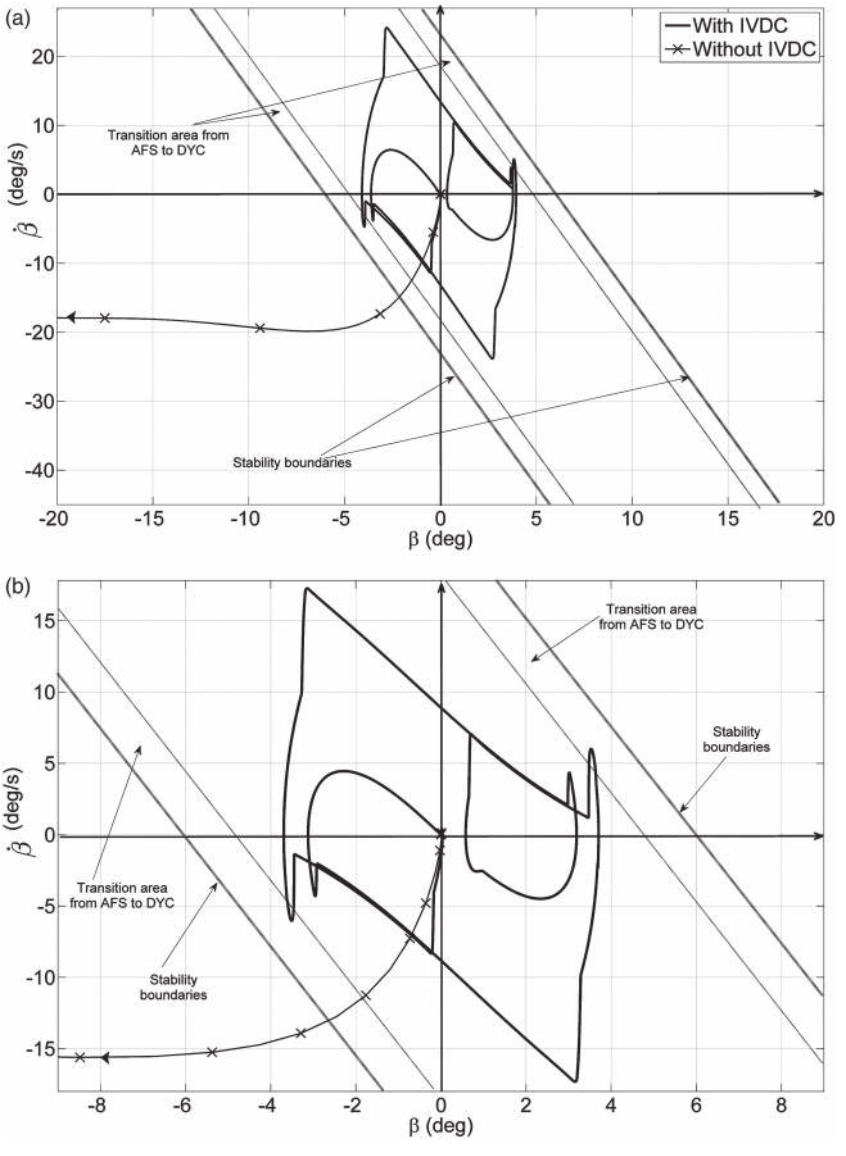

Figure 14. (a) $\beta - \dot{\beta}$ phase plane – dry road. (b). $\beta - \dot{\beta}$ phase plane – wet road.

steady-state response at around the fifth second of the simulation time; however, the transient response of the system controlled by the NFTSM method reaches the steady-state response at the first second of the simulation time and with no overshoot. The comparison between these two SMC methods to control the front wheel angle generated by the front wheel subsystem of the steer-by-wire system can be referred from [44].

Consequently, it is proved that the NFTSM control strategy with the assistance of the ITSM control method enhances the yaw rate tracking controller's transient response, which is faster than the response of the system controlled by the SMC strategy.

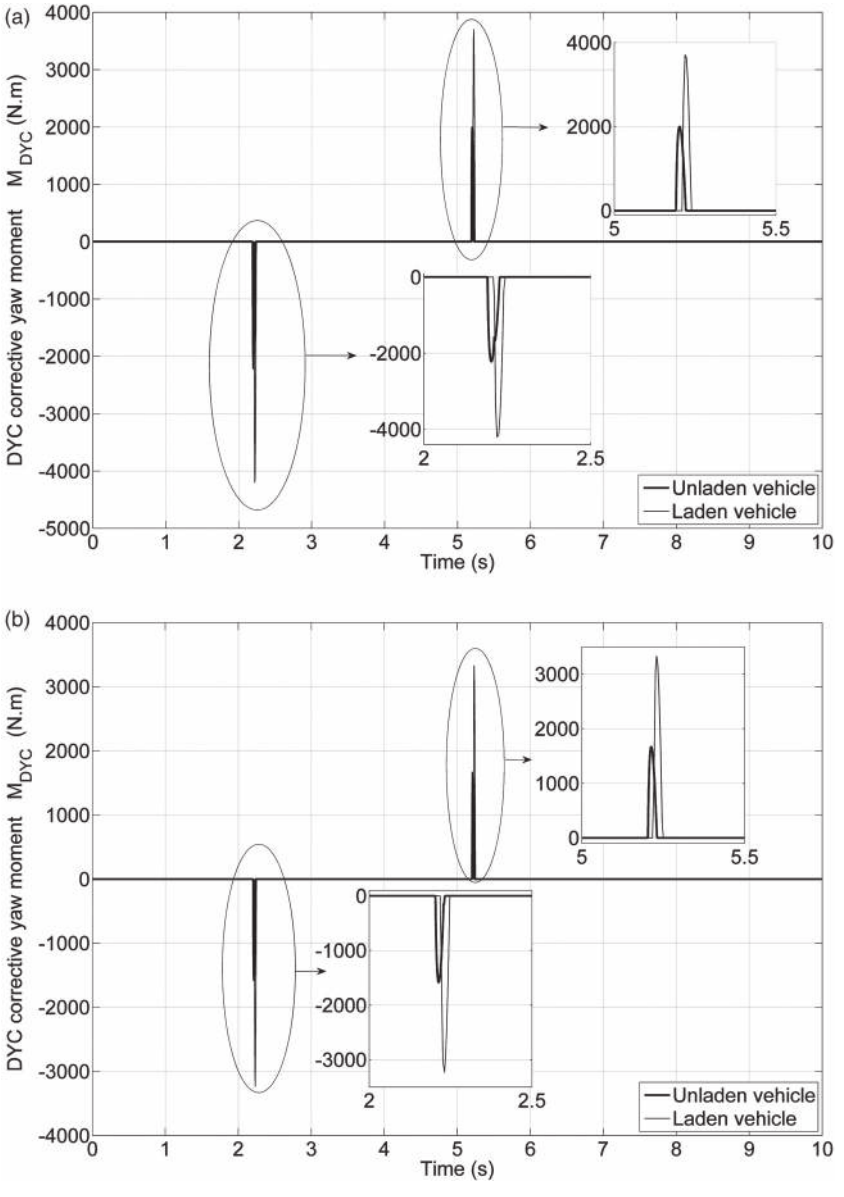

Figure 15. (a) DYC corrective yaw moment – dry road. (b). DYC corrective yaw moment – wet road.

6. Conclusion and future work

The major contribution of this paper is in implementing two advanced types of terminal SMC methods, ITSM and NFTSM, in an IVDC strategy by way of involving AFS using a steer-by-wire actuator and DYC utilising a differential braking system to improve handling and stability of a ground vehicle in fast and finite time performance. To organise the integration of AFS and DYC into IVDC, a phase plane diagram based on the stability index function of the sideslip dynamics is employed. In this integration mechanism, the AFS system can be adopted in the stable condition to enhance the handling, while AFS and DYC

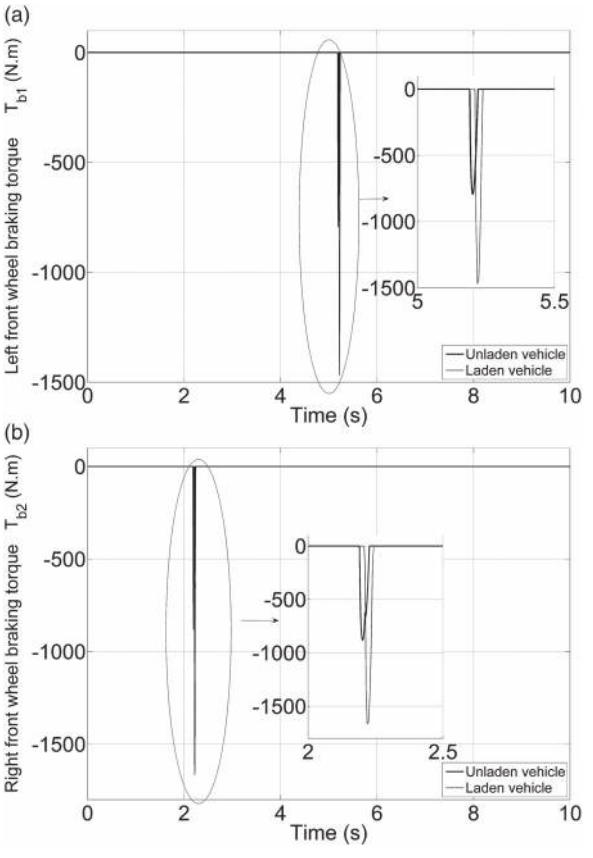

Figure 16. (a) Left front wheel braking torque – dry road. (b). Right front wheel braking torque – dry road.

act together in the unstable dynamic situation, when AFS loses its ability to stabilise the vehicle. The effectiveness of the proposed control scheme including IVDC, SbW, and differential braking systems is evaluated by simulation results for an 8-DOF nonlinear vehicle model in some critical manoeuvres. Simulations conducted under various adverse driving conditions show that the overall system developed in this study significantly enhances the transient response of the control system and also reduces the chattering phenomenon when the system operates close to the sliding surface. In addition the proposed control system demonstrates good robustness against uncertain parameters and external disturbance, and excellent tracking performance.

As the weighting coefficients in Equation (34) have been found through a trial and error method in order to combine the AFS stand-alone controllers, the next research stage will focus on integration of the AFS stand-alone controllers using the control allocation technique. Also implementation of ABS can improve the differential braking system in order to avoid the tyre being locked if the braking torques exceed their physical limits. In addition, research on consideration of the actuators constraints and also sideslip angle estimator could further enhance the suitability of the proposed control structure for modelling of real-time control aspects. Moreover, this study can be further improved through

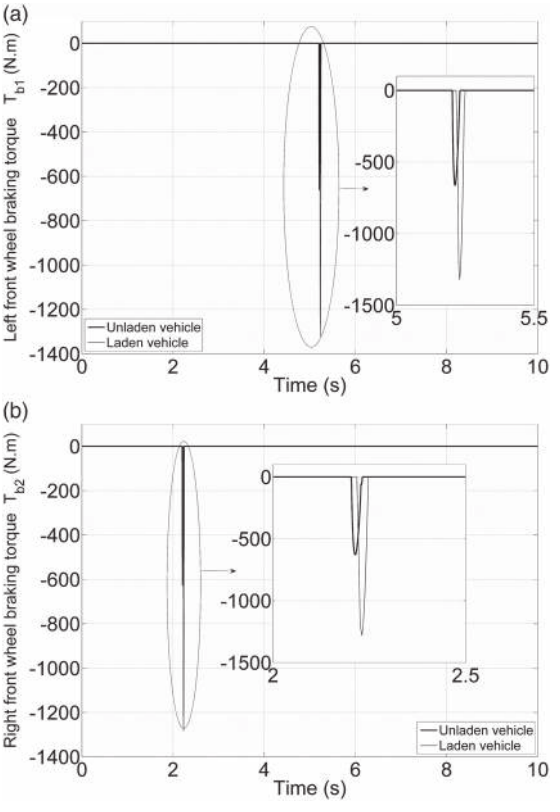

Figure 17. (a) Left front wheel braking torque – wet road. (b). Right front wheel braking torque – wet road.

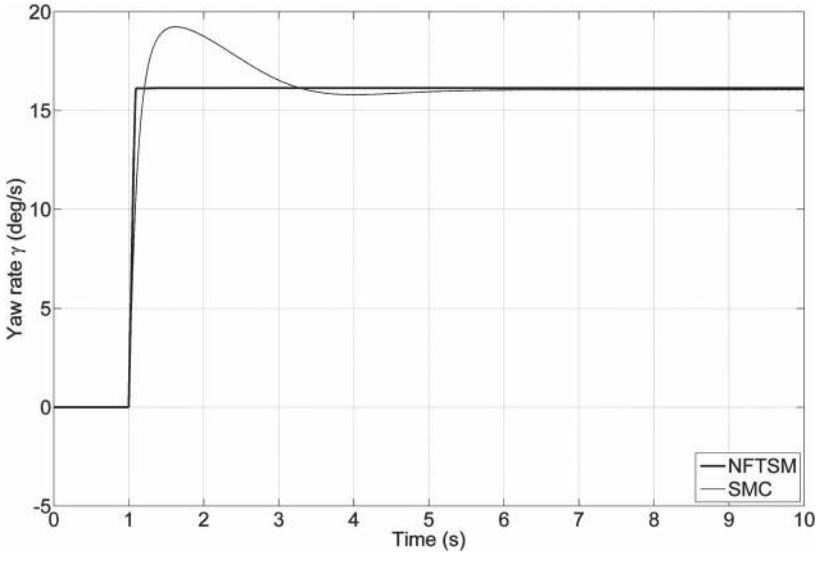

Figure 18. Comparison of the conventional SMC and NFTSM.

the implementation of the proposed control structure on vehicles for experimental testing in a real time.

Disclosure statement

No potential conflict of interest was reported by the authors.

References

[1] Wong JY. Theory of ground vehicles. 3rd ed. New York: John Wiley & Sons; 2001.
[2] Kawaguchi Y, Eauchi H, Osuka K. Passivity-based adaptive nonlinear control for active steering. Proceedings of the 16th IEEE international conference on control applications; Singapore; 2007.
[3] Falcone P, Borrelli F, Tseng HE, Asgari J, Hrovat D. Linear time-varying model predictive control and its application to active steering systems: stability analysis and experimental validation. Int J Robust Nonlinear Control. 2008;18(8):862–875.
[4] Zhang JY, Kim JW, Lee KB, Kim YB. Development of an active front steering (AFS) system with QFT control. Int J Autom Technol. 2008;18(8):862–875.
[5] Ohara H, Murakami T. A stability control by active angle control of front-wheel in a vehicle system. IEEE Trans Ind Electron. 2008;55(3):1277–1285.
[6] Zheng B, Anwar S. Yaw stability control of a steer-by-wire equipped vehicle via active front wheel steering. Mechatronics. 2009;19(6):799–804.
[7] Mousavinejad I, Kazemi R. Variable structure controller design for steer-by-wire system of a passenger car. J Mech Sci Technol. 2014;28(8):3285–3299.
[8] Nam K, Fujimoto H, Hori Y. Lateral stability control of in-wheel-motor-driven electric vehicles based on sideslip angle estimation using lateral tire force sensors. IEEE Trans Veh Technol. 2012;61(5):1972–1985.
[9] Hirano Y, Fukatani K. Development of robust active rear steering control for automobile. JSME Int J C: Dyn Control. 1997;40(2):231–238.
[10] Zheng S, Tang H, Han Z, Zhang Y. Controller design for vehicle stability enhancement. Control Eng Pract. 2006;14(12):1413–1421.
[11] Esmailzadeh E, Goodarzi A, Vossoughi GR. Optimal yaw moment control law for improved vehicle handling. Mechatronics. 2003;13(7):659–675.
[12] Anwar S. Generalized predictive control of yaw dynamics of a hybrid brake-by-wire equipped vehicle. Mechatronics. 2005;15(9):1089–1108.
[13] Kim D, Hwang S, Kim H. Vehicle stability enhancement of four-wheel-drive hybrid electric vehicle using rear motor control. IEEE Trans Veh Technol. 2008;57(2):727–735.
[14] Zhou H, Liu Z. Vehicle yaw stability-control system design based on sliding mode and backstepping control approach. IEEE Trans Veh Technol. 2010;59(7):3674–3678.
[15] Choi M, Choi SB. Model predictive control for vehicle yaw stability with practical corners. IEEE Trans Veh Technol. 2014;63(8):3539–3548.
[16] Aripin MK, Sam YM, Danapalasingam KA, Peng K, Hamzah N, Ismail MF. A review of active yaw control system for vehicle handling and stability enhancement. Int J Veh Technol. 2014;2014(437515):1–15.
[17] Abe M. Trends of intelligent vehicle dynamics control and their future. Rep. 81. Kanagawa Institute of Technology; 2013.
[18] Selby MA, Manning WJ, Crolla DA, Brown MD. A comparison of the relative benefits of active front steering and active rear steering when coordinated with direct yaw moment control. Proceedings of ASME international mechanical engineering congress and exposition, New York; 2001.
[19] Gordon T, Howell M, Brandao F. Integrated control methodologies for road vehicles. Veh Syst Dyn. 2003;40(1–3):157–190.
[20] Yu F, Li D-F, Crolla DA. Integrated vehicle dynamics control – state-of-the art review. Proceedings of the IEEE vehicle power and propulsion conference, Harbin; 2008.

[21] Yang X, Wang Z, Peng W. Coordinated control of AFS and DYC for vehicle handling and stability based on optimal guaranteed cost theory. Veh Syst Dyn. 2009;47(1):57–79.
[22] Li D, Du S, Yu F. Integrated vehicle chassis control based on direct yaw moment, active steering and active stabilizer. Veh Syst Dyn. 2008;46(1):341–351.
[23] Zhang B-L, Han Q-L, Zhang X-M, Yu X. Integral sliding mode control for offshore steel jacket platforms. J Sound Vib. 2012;331(14):3271–3285.
[24] Zhang B-L, Ma L, Han Q-L. Sliding mode H_∞ control for offshore steel jacket platforms subject to nonlinear self-excited wave force and external disturbance. Nonlinear Anal-Real World Appl. 2013;14(1):163–178.
[25] Zhang B-L, Han Q-L, Zhang X-M, Yu X. Sliding mode control with mixed current and delayed states for offshore steel jacket platforms. IEEE Trans Control Syst Technol. 2014;22(5):1769–1783.
[26] Baslamish SC, Kose IE, Anlas G. Handling stability improvement through robust active front steering and active differential control. Veh Syst Dyn. 2011;49(5):657–683.
[27] Baslamish SC, Kose IE, Anlac G. Gain-scheduled integrated active steering and differential control for vehicle handling improvement. Veh Syst Dyn. 2009;47(1):99–119.
[28] Baslamish SC, Kose IE, Anlac G. Design of active steering and intelligent braking systems for road vehicle handling improvement: a robust control approach. Proceedings of the 2006 IEEE international conference on control applications, Munich; 2006.
[29] Di Cairano S, Tsengz HE. Driver-assist steering by active front steering and differential braking: design, implementation and experimental evaluation of a switched model predictive control approach. Proceedings of the 49th IEEE conference on decision and control, Atlanta; 2010.
[30] Falcone P, Tseng HE, Borrelli F, Asgari J, Hrovat D. MPC-based yaw and lateral stabilization via active front steering and braking. Veh Syst Dyn. 2008;46(1):611–628.
[31] Tjonnas J, Johansen TA. Stabilization of automotive vehicles using active steering and adaptive brake control allocation. IEEE Trans Control Syst Technol. 2010;18(3):545–558.
[32] Wu J, Wang Q, Wei X, Tang H. Studies on improving vehicle handling and lane keeping performance of closed-loop driver-vehicle system with integrated chassis control. Math Comput Simul. 2010;80(12):2297–2308.
[33] Doumiati M, Sename O, Dugrad L, Martinez-Molina JJ, Gaspar P, Szabo Z. Integrated vehicle dynamics control via coordination of active front steering and rear braking. Eur J Control. 2013;19(2):121–143.
[34] Mousavinejad I, Zhu Y, Vlacic L. Control strategies for improving vehicle stability, state-of-the-art review. Proceedings of the 10th Asian control conference, Kota Kinabalu; 2015.
[35] Yang L, Yang J. Nonsingular fast terminal sliding-mode control for nonlinear dynamical systems. Int J Robust Nonlinear Control. 2011;21(16):1865–1879.
[36] Khoo S, Xie L, Man Z. Integral terminal sliding mode cooperative control of multi-robot networks. Proceedings of the 2009 IEEE/ASME international conference on advanced intelligent mechatronics, Singapore; 2009.
[37] Inagaki S, Kushiro I, Yamamoto M. Analysis on vehicle stability in critical cornering using phase-plane method. JSAE Rev. 1995;16(2):287–292.
[38] Selby. Intelligent vehicle motion control [PhD diss.]. Mechanical Engineering Department, University of Leeds, Leeds; 2003.
[39] Jazar RN. Vehicle dynamics, theory and application. 2nd ed. New York: Springer; 2014.
[40] Rajamani R. Vehicle dynamics and control. 2nd ed. New York: Springer; 2012.
[41] Abe M, Kato A, Suzuki K, Kano Y. Estimation of vehicle side-slip angle for DYC by using on-board-tire-model. Proceedings of the 4th international symposium on advanced vehicle control, Nagoya; 1998.
[42] He J, Crolla DA, Levesley MC, Manning WJ. Coordination of active steering, driveline, and braking for integrated vehicle dynamics control. Proc Int Mech Eng D: J Autom Eng. 2006;220(10):1401–1420.
[43] Pacejka HB. Tyre and vehicle dynamics. 3rd ed. Oxford: Butterworth-Heinemann; 2012.
[44] Mousavinejad I, Zhu Y, Vlacic L. Nonsingular fast terminal sliding mode control approach to front wheel subsystem of steer-by-wire system. Proceedings of the 5th Australian control conference, Gold Coast; 2015.